Optics Letters

Axicon-based Bessel beams for flat-field illumination in total internal reflection fluorescence microscopy

Benjamin Schreiber,[1,2] Kareem Elsayad,[2] and Katrin G. Heinze[1,*]

[1]Rudolf Virchow Center, Research Center for Experimental Biomedicine, University of Würzburg, Josef-Schneider-Str. 2, 97080 Würzburg, Germany
[2]Advanced Microscopy Facility, Vienna Biocenter Core Facilities, Dr. Bohr-Gasse 3, A-1030 Vienna, Austria
*Corresponding author: katrin.heinze@virchow.uni-wuerzburg.de

Received 31 July 2017; revised 31 August 2017; accepted 1 September 2017; posted 6 September 2017 (Doc. ID 303364); published 25 September 2017

Total internal reflection fluorescence microscopy (TIRF-M) provides low-invasive high-contrast surface imaging with optical sectioning of typically 100–200 nm. Thus, TIRF-M has become an established tool for imaging surfaces, including cell membranes. For TIRF-M, a homogenous evanescent field of excitation over the whole field of view is generally desired for quantitative microscopy; however, this is not necessarily straightforward to generate with Gaussian beams. In recent years, several improvements on TIRF-M have been developed that have addressed non-uniform scattering fringes and other artifacts. Here, we introduce a cost-effective TIRF setup with a very low degree of complexity and no moving parts, which provides a flattop-like excitation profile. The setup uses a tunable laser ring zoom focus system to generate a full 360° TIRF illumination. Two axicon lenses and one focus lens allow for generation and control of the ring diameter to tune the TIRF excitation angle. We show that 360° laser illumination in combination with a radial polarizer will generate an evanescent Bessel-beam excitation field that exhibits a flattop intensity over an extended part of the field of view, and demonstrate the advantages of this axicon-based Bessel beam illumination for live-cell imaging. © 2017 Optical Society of America

OCIS codes: (170.2945) Illumination design; (110.0180) Microscopy; (180.2520) Fluorescence microscopy; (260.6970) Total internal reflection.

https://doi.org/10.1364/OL.42.003880

Total internal reflection fluorescence microscopy (TIRF-M) has become a key technique in the life sciences and allows for fast high-contrast fluorescence imaging in the cell membrane region. Fluorescent dyes in close vicinity (up to a few hundred nanometers) to the microscopy cover slip interface are selectively excited by an evanescent field. The steep exponential axial intensity decay prevents out-of-focus fluorescence excitation [1]. Focusing a single Gaussian laser beam off-centered onto the objective back focal plane (BFP) is the most common way to achieve an evanescent excitation field in TIRF microscopes [2]. This results in an inevitable and generally undesirable lateral asymmetry of the excitation field that can hardly be avoided in this otherwise elegant and simple approach, as the single laser beam has to be focused at the periphery of the objective rear aperture to ensure overcritical angle illumination. Since homogenous excitation over the whole field of view (FOV) is crucial for many applications, several TIRF improvements have been developed over the last century. Popular approaches for enhanced field homogeneity are based on 360° incoherent illumination [3,4], variable-angle TIRF (VATIRF) [5], and spinning TIRF (sp-TIRF) [6–8]. Such approaches result in a radial symmetric Gaussian illumination field for TIRF microscopes and suppress shadowing and TIRF fringe artifacts caused by one-sided illumination. To achieve a homogenous flattop illumination field, the combination of single and multimode fibers [9] or micro-lens arrays [10] can be used. Those allow a flat-field homogenous epi-fluorescence wide-field illumination with great potential to improve single-molecule imaging. Unfortunately, these flat-field approaches have not been applied to TIRF-M.

Our work presented here closes this gap, as we introduce an objective-based homogeneous TIRF illumination using Bessel-beam side lobes. Bessel beams have become highly desired and well-studied microscopy tools, as they concentrate a large amount of laser intensity in a sub-diffractive limited laser spot [11]. Bessel-beam illumination has been well known in the fluorescence microscopy community for decades and has been successfully implemented in structural illumination and light-sheet microscopy [12–14]. For our approach, a radial symmetric evanescent field is formed at the microscopy coverslip-sample interface by 360° overcritical p-polarized illumination. Focusing a radially polarized laser ring at the TIRF objective BFP ensured all-sided p polarization. The resulting intensity distribution in the image plane is described by a squared zero order Bessel function with an exponential intensity decay in axial direction [15]. It has been previously shown that the resulting evanescent subdiffraction limited spot can be used for

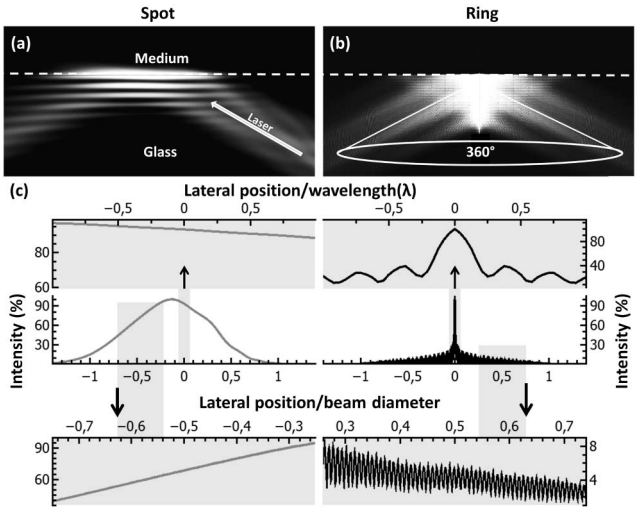

Fig. 1. Finite elements method calculations for single-spot Gaussian (a) and 360° ring TIR illumination (b). Corresponding lateral intensity cross sections at the glass-to-medium interface (c). The middle row shows cross-section overviews. Gray boxes indicate corresponding regions of interest and zoom-in at the center region (top) and at the side-lope region (bottom) as indicated.

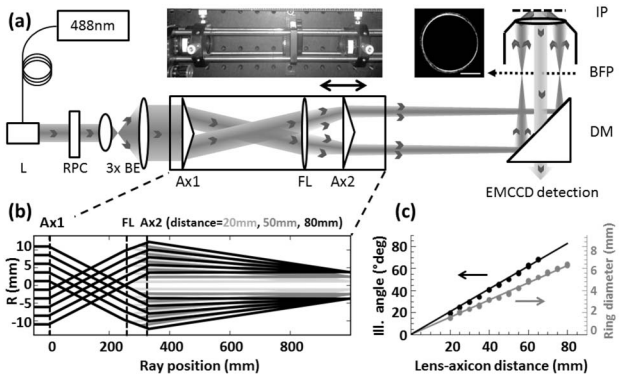

Fig. 2. AxiTIRF-M with laser ring focus system. Illustration of optical design (a) with photograph (middle) and the inset image of the laser ring back reflection (right, scale bar 2 mm) inset. Main optical components are laser (L), radial polarization converter (RPC), beam expander (BE), two axicons (Ax1 and Ax2), focus lens (FL), and a dichroic mirror (DM). Objective back focal and image plane (BFP and IP) are indicated. Ray traces of AxiTIRF-M for 20 mm, 50 mm, and 80 mm lens-axicon distances (b). Measured illumination angle and ring diameter (at BFP) (c), depending on lens-axicon distance.

single spot TIRF-STED-FCS (stimulated emission depletion–fluorescence correlation spectroscopy) [16]. In this work, we demonstrate that Bessel-beam side lobes also have potential for homogenous and flattop-like TIRF illumination.

Figure 1 shows finite element method calculations (*COMSOL Multiphysics 4.4*) for a typical single-spot Gaussian illumination (a) and radially polarized 360° Gaussian ring illumination (b) for an excitation wavelength of 488 nm and an illumination angle of 63°. The corresponding maximum normalized intensity distributions at the glass–sample interface ($RI = 1.52/1.33$) are plotted below (c). Note that the x axis in (c) was normalized to the excitation wavelength and beam diameter of 10 μm.

The overcritical single spot illumination shows the typical Gaussian behavior. As expected, only at the center of the FOV is the intensity distribution homogenous. It is this relatively small area that is typically used in TIRF-M and spectroscopy. This area can be extended by the size of the incoming laser beam if reduced laser intensity is experimentally acceptable. The rest of the lateral excitation field is noticeably asymmetric along the direction of the excitation beam, and the maximum intensity is shifted from the center of the focus. This is caused by the illumination angle tilted projection of the incoming Gaussian beam. Thus, for Gaussian-illuminated side areas, the intensity drops from the higher center area to the background level, which is challenging when quantitative imaging and/or low-light applications have to be performed.

On the contrary, a 360° radially polarized laser excitation results in evanescent illumination and a radial-symmetric zero-order Bessel function in the lateral plane [15]. Radial polarization ensures that the radial symmetric evanescent field is fed by all-sided *p*-polarized illumination. Figure 1(b) shows respective illumination simulations with corresponding intensity line plots (panel *c*, right). Here, the Bessel-beam center exhibits the typical sub-diffractive intensity spot with a full width at half-maximum (FHWM) of 0.32λ and the first intensity minimum at 0.26λ. The Bessel-beam side lobes show an interference pattern with a shallower radial intensity gradient than in the Gaussian case. The simulations demonstrate the potential of evanescently generated Bessel beams for improved objective-based TIRF-M. We favor an objective-based configuration, as this is often advantageous in cell imaging compared to the prism-based TIRF-M. In the objective-type method, the specimen is well accessible, and the angle of incidence of the laser light can be changed easily.

Figure 2 shows the experimental setup (a) and calibration (b) and (c) to generate a 360° ring illumination in our TIRF-M. The illumination part of the setup is largely inspired by Dickey and co-workers' annular laser ring zoom system [17] with several important variations. The illumination profile is generated by the use of axicons (cone lenses) and a focus lens. More specifically, a first axicon (Ax1) forms the laser ring, which is subsequently focused by the focus lens (FL). A second axicon (Ax2) then neutralizes the deflection of the laser beam and determines the ring diameter of the laser ring zoom system. The ring diameter control of the laser focused at the objective lens BFP is the crucial feature to finally control the TIR illumination angle.

In our setup, two 5° axicon lenses (AX255-A, Thorlabs) and a focus lens ($f = 750$ mm, LA1978-A, Thorlabs) are used to control this. First, a single-mode fiber (NA 0.11) coupled laser diode (06-MLD 488 nm, Cobolt) with a reflective collimator (RC08APC-P01, Thorlabs) was used to create an 8 mm laser output. The beam was then passed through a radial polarization converter (RPC) consisting of a $\lambda/2$ waveplate (AHWP05M-600, Thorlabs) and *s*-waveplate (RPC-488-08, Altechna) generating a radially polarized laser beam. A beam expander (3×) optimized the performance of the first axicon in the AxiTIRF-M. Note that the first axicon and the focus lens are separated by 250 mm [see Fig. 2(b)]. The resulting radially polarized laser ring is focused at the TIRF objective BFP. A dichroic mirror (Beamsplitter HC BS 500, *AHF* Analysentechnik) was used for

light filtering and coupling to the microscope stand (IX73, Olympus), which was equipped with a TIRF objective (APON 100XHOTIRF, Olympus, NA: 1.7) suitable for TIR illumination and fluorescence collection. AxiTIRF imaging can also be obtained with standard TIRF objectives. Here, we used the NA 1.7 objective to allow TIRF-M in Mowiol-mounted samples where the refractive index difference to glass is usually not sufficient to perform TIRF-M with more common (NA ~ 1.49) TIRF objectives. This optical layout allows for a theoretical FOV of 28.8 μm. For direct comparison with single-spot illumination, the axicons can be removed from the light path and replaced by a tiltable glass plate (thickness: 10 mm) to laterally displace the focus at the BFP. An iris diaphragm ensures a comparable total FOV for single-spot and ring illumination. The collected fluorescence is filtered by a bandpass (525/50, *AHF* Analysentechnik) magnified by 2.5 and focused onto an EMCCD (iXon^{EM} + DU-897D, Andor Technology Ltd.).

Figure 2(b) shows two-dimensional ray-trace calculations of the realized AxiTIRF-M with lens-axicon separations of 20 mm, 50 mm, and 80 mm. By separating the lens axicon, the diameter of the laser ring focus increases linearly [see Fig. 2(c)]. Linear-fitted slopes for ring diameter and illumination angle over the lens-axicon distance are 0.039 and 1.03 (°/mm), respectively. Penetration depths of the setup were determined by 6 μm FocalCheck Microspheres (F14808, Invitrogen, for the method, see, e.g., [18]).

Next, we demonstrate AxiTIRF-M for fluorescent imaging of cells. The cells were stained for actin filaments (f-actin) fluorescently labeled with AlexaFluor488 (A488)-Phalloidin (Invitrogen). Wild-type Chinese hamster ovary (CHO) cells were cultured at 37°C and 5% CO_2 in Dulbecco's Modified Eagle Medium (DMEM/F12, Thermofischer). Cells were grown and seeded on high refractive index ($RI = 1.78$) NLAFN-21 cover slips (150 μm thick, UQG Optics Ltd.). Note that high refractive index cover slips were used even to allow for TIRF imaging of Mowiol-mounted cells; respective live cell experiments would not require special coverslips. Before imaging, cells were paraformaldehyde fixed (4%) for 10 min, permeabilized by 1% Triton X-100 (Sigma-Aldrich) for 5 min, and stained with A488-Phalloidin (1:200) for 30 min at room temperature and mounted in Mowiol 4-88 (Sigma-Aldrich). For imaging, a laser (Cobolt 06-MLD 488 nm, set laser power: 0.4 mW continuous wave emission) and an EMCCD camera were used (gain: 300; exposure time: 100 ms). For AxiTIRF imaging, a lens-axicon distance of 67°–72° incident angle (corresponding to lens-axicon distances of 65–70 mm) was found to be optimal and used in all cell experiments. The measured effective excitation penetration depth was 220 ± 30 nm.

Figure 3 shows cell images for wide-field (a) and conventional TIRF mode (b). The corresponding fluorescence intensity line plot is plotted in (c). For a small ring diameter (lens-axicon distance = 20 mm) cells are illuminated in wide-field mode [see Fig. 3(a)]. With increasing the lens-axicon distance, the illumination angle finally overcomes the critical angle for proper TIRF illumination [see Fig. 3(b)]. As expected, the wide-field image shows out-of-focus fluorescence background, particularly in the center of the FOV, while in over-critical TIRF illumination, out-of-focus background in this center area and beyond is reduced [see Fig. 3(c)]. For a selected

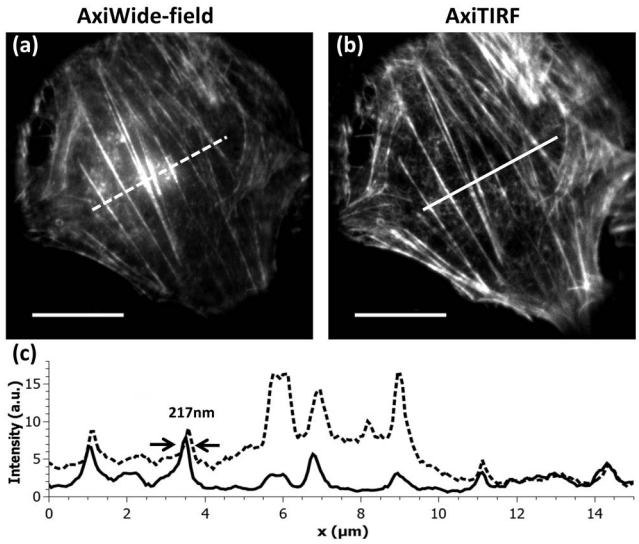

Fig. 3. Comparison of ring-illuminated AxiWide-field (a) and AxiTIRF images (b) of A488-Phalloidin labeled CHO cells. Corresponding fluorescence intensity cross sections (c). Scale bars: 10 μm.

f-actin, a FWHM of 217 nm was measured to estimate the lateral resolution of the setup.

Next, we compare single-spot Gaussian TIRF-M and AxiTIRF-M (see Fig. 4) for both 1 μM A488 dye solution (a) with the corresponding line scans plotted in (b). Images of CHO cells stained for A488-Phalloidin (see above) are

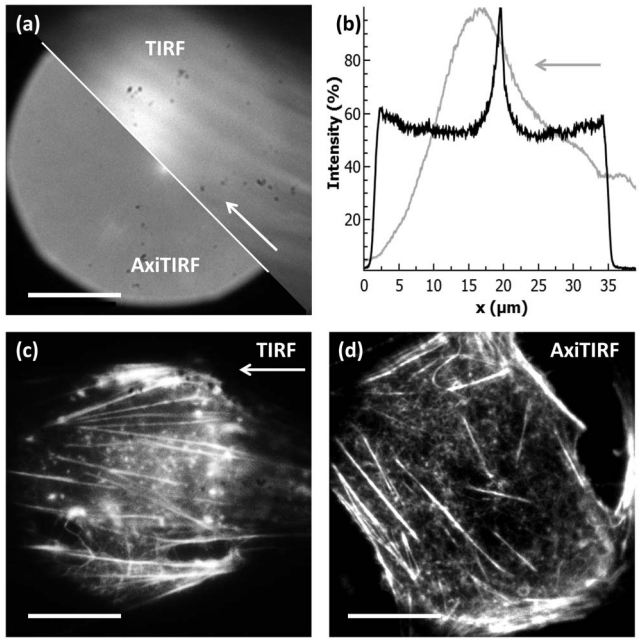

Fig. 4. A488 dye solution (a) imaged for direct single-spot TIRF and AxiTIRF illumination field comparison with corresponding fluorescence intensity cross sections (b). Comparison of single-spot TIRF (c) and AxiTIRF-M images (d) of A488-Phalloidin labeled CHO cells. Arrows indicate the direction of single-spot illumination. Scale bars: 10 μm.

shown in (c)–(d). For AxiTIRF-M, a symmetric flattop-like illumination with the zero-order center spot is achieved. In contrast, the single-spot illumination follows the classical Gaussian distribution with its asymmetry due to the static excitation direction [see arrows in Figs. 4(a) and 4(c)]. The measurements are in good agreement with finite element method calculations, shown in Fig. 1. For the cell images, we note a background suppression in both classic and AxiTIRF-M; however, there is one striking difference: for single side illumination, the images show an asymmetric and inhomogeneous intensity distribution and effectively exhibit three subareas—first, the well-illuminated middle part, second, a fast decaying shoulder at the opposite side of the illumination direction, and, third, a slower decaying shoulder at the excitation side. Consequently the classic TIRF image is dimmer at the periphery with the most pronounced effects at the side farthest from illumination direction. In contrast, the AxiTIRF-M image in Fig. 4(d) is homogeneously illuminated with an effectively increased FOV (26.2 ± 0.12 μm for TIRF-M derived from Gaussian fit with linear background, and 31.2 ± 0.1 μm for AxiTIRF-M derived from plateau width).

Note that for the cell sample, we could observe neither a clear bright center peak nor any disturbing Bessel beam side lobes, most likely due to regular (elastic/Rayleigh) scattering and loss of coherence (and this vanishing interference), which feeds the Bessel-beam spot. Another reason may be due to the inhomogeneity of the sample [19] or cover-slip–sample interface, which may smooth the interference effect. In Fig. 4(a) we noticed some weak shadowing stripes aligned radially to the illumination center. Excitation through a multi-mode fiber may allow for suppression of such weak interference patterns [3], but may compromise the sharp Bessel form formation.

In conclusion, we have shown that an axicon-based laser ring focused on a TIRF objective BFP can be used for TIRF-M with added value. The resulting Bessel beam effectively enlarges the FOV and provides a homogeneous TIRF illumination in a cell-friendly objective-based setup. The laser ring diameter can be easily adjusted by moving one lens along the optical axis, which allows for switching between wide-field and TIRF mode. AxiTIRF-M increases the effective FOV in comparison to classic TIRF-M by almost a factor of two, as the radially polarized laser ring generates an evanescent flattop illumination around a narrow center spot. Thus, the FOV for AxiTIRF-M becomes remarkably big compared to standard single-spot Gaussian illumination where just a few percent of the central area is homogenously illuminated.

We believe that the illumination scheme of AxiTIRF-M has great potential for single-molecule tracking and localization applications where a homogenous illumination over few μm FOV is desirable. Since the illumination strategy is based on a radial symmetric illumination, we can imagine that this ring illumination could also have potential for TIRF structured illumination microscopy (SIM) when the laser ring is chopped into two segments with a rotatable slit mask. As discussed by Chung *et al.* [20], even more pairs of interfering laser beams can be used for SIM TIRF with an increased point spread function symmetry. With some additional tweaks, the setup described here is also potentially suitable for 360° incoherent illumination, which would further suppress TIRF fringes and would allow for even shadowless TIRF-M.

Funding. Elitenetzwerk Bayern (K-BM-2013-247).

Acknowledgment. B. S. and K. H. are supported by the International Doctoral Program (IDK) Receptor Dynamics: Emerging Paradigms for Novel Drugs of the ENB. K. E. acknowledges support from the City of Vienna and the Austrian Ministry of Science. We thank Hannah Heil and Kerstin Jansen for assistance with cell culture, and all members of the Advanced Microscopy Facility of AdvMicro for fruitful discussions.

REFERENCES

1. D. Axelrod, Traffic **2**, 764 (2001).
2. D. Axelrod, Methods Cell Biol. **89**, 169 (2008).
3. M. Lei and A. Zumbusch, Opt. Lett. **35**, 4057 (2010).
4. J. Lin and A. D. Hoppe, Microsc. Microanal. **19**, 350 (2013).
5. M. van't Hoff, V. de Sars, and M. Oheim, Opt. Express **16**, 18495 (2008).
6. K. L. Ellefsen, J. L. Dynes, and I. Parker, PLoS ONE **10**, e0136055 (2015).
7. A. L. Mattheyses, K. Shaw, and D. Axelrod, Microsc. Res. Tech. **69**, 642 (2006).
8. R. Fiolka, Y. Belyaev, H. Ewers, and A. Stemmer, Microsc. Res. Tech. **71**, 45 (2008).
9. J. Deschamps, A. Rowald, and J. Ries, Opt. Express **24**, 28080 (2016).
10. K. M. Douglass, C. Sieben, A. Archetti, A. Lambert, and S. Manley, Nat. Photonics **10**, 705 (2016).
11. J. Durnin, J. J. Miceli, and J. H. Eberly, J. Opt. Soc. Am. A **3**, 128 (1986).
12. L. Gao, L. Shao, B.-C. Chen, and E. Betzig, Nat. Protoc. **9**, 1083 (2014).
13. B. C. Chen, W. R. Legant, K. Wang, L. Shao, D. E. Milkie, M. W. Davidson, C. Janetopoulos, X. S. Wu, J. A. Hammer III, Z. Liu, B. P. English, Y. Mimori-Kiyosue, D. P. Romero, A. T. Ritter, J. Lippincott-Schwartz, L. Fritz-Laylin, R. D. Mullins, D. M. Mitchell, J. N. Bembenek, A. C. Reymann, R. Bohme, S. W. Grill, J. T. Wang, G. Seydoux, U. S. Tulu, D. P. Kiehart, and E. Betzig, Science **346**, 1257998 (2014).
14. T. Vettenburg, H. I. Dalgarno, J. Nylk, C. Coll-Llado, D. E. Ferrier, T. Cizmar, F. J. Gunn-Moore, and K. Dholakia, Nat. Methods **11**, 541 (2014).
15. D. Axelrod, Biophys. J. **104**, 1401 (2013).
16. M. Leutenegger, C. Ringemann, T. Lasser, S. W. Hell, and C. Eggeling, Opt. Express **20**, 5243 (2012).
17. F. M. Dickey and J. D. Conner, Proc. SPIE **8130**, 81300B (2011).
18. K. N. Fish, in *Current Protocols in Cytometry* (Wiley, 2009), pp. 12.18.1–12.18.13.
19. J. Beuthan, O. Minet, J. Helfmann, M. Herrig, and G. Muller, Phys. Med. Biol. **41**, 369 (1996).
20. E. Chung, D. Kim, Y. Cui, Y. H. Kim, and P. T. C. Soy, Biophys. J. **93**, 1747 (2007).

193.171.188.3 {ts '2018-12-06 04:27:18'}